Published in final edited form as:
Biofabrication. 2012 September ; 4(3): 035005. doi:10.1088/1758-5082/4/3/035005.

Rapid 3D printing of anatomically accurate and mechanically heterogeneous aortic valve hydrogel scaffolds

L A Hockaday[1], **K H Kang**[1], **N W Colangelo**[1], **P Y C Cheung**, **B Duan**[1], **E Malone**[2], **J Wu**[1], **L N Girardi**[4], **L J Bonassar**[1,2], **H Lipson**[2], **C C Chu**[3], and **J T Butcher**[1,2]

[1]Department of Biomedical Engineering, Cornell University, Ithaca, NY, USA

[2]Sibley School of Mechanical and Aerospace Engineering, Cornell University, Ithaca, NY, USA

[3]Department of Fiber Science and Apparel Design, Cornell University, Ithaca, NY, USA

[4]Department of Cardiothoracic Surgery, Weill Cornell Medical College, New York City, NY, USA

Abstract

The aortic valve exhibits complex three-dimensional (3D) anatomy and heterogeneity essential for long-term efficient biomechanical function. These are, however, challenging to mimic in *de novo* engineered living tissue valve strategies. We present a novel simultaneous 3D-printing/photocrosslinking technique for rapidly engineering complex, heterogeneous aortic valve scaffolds. Native anatomic and axisymmetric aortic valve geometries (root wall and tri-leaflets) with 12 to 22 mm inner diameters (ID) were 3D printed with poly-ethylene glycol-diacrylate (PEG-DA) hydrogels (700 or 8000 MW) supplemented with alginate. 3D printing geometric accuracy was quantified and compared using Micro-CT. Porcine aortic valve interstitial cells (PAVIC) seeded scaffolds were cultured for up to 21 days. Results showed that blended PEG-DA scaffolds could achieve over 10-fold range in elastic modulus (5.3±0.9 to 74.6±1.5 kPa). 3D printing times for valve conduits with mechanically contrasting hydrogels were optimized to 14 to 45 minutes, increasing linearly with conduit diameter. Larger printed valves had greater shape fidelity (93.3±2.6, 85.1±2.0, and 73.3±5.2% for 22, 17, and 12 mm ID porcine valves; 89.1±4.0, 84.1±5.6, and 66.6±5.2% for simplified valves). PAVIC seeded scaffolds maintained near 100% viability over 21 days. These results demonstrate that 3D hydrogel printing with controlled photocrosslinking can rapidly fabricate anatomical heterogeneous valve conduits that support cell engraftment.

1. Introduction

Aortic valve disease (AVD) is a serious and increasing clinical burden that affects patients at all stages and walks of life. In particular, congenital heart valve defects, which affect 1-2% of all live births in the United States, predispose the valve to premature failure and can be fatal if left untreated (Hoffman and Kaplan 2002). AVD is most commonly treated with surgical replacement of the defective valve. Tissue engineering has the potential to address current limitations of non-living prosthetics and donor supply shortage of allografts by providing living tissues that can grow, remodel, and integrate with the patient (Butcher, Mahler et al. 2011).

A major criterion for a tissue engineered heart valve is that the engineered valve must mimic the physiological function of the native valve. Several studies highlight that the natural geometry of the root, cusps, and sinus wall is critical for enabling efficient hemodynamics

jtb47@cornell.edu.

and coronary flow (Bellhouse, Bellhouse et al. 1968; Vesely 2000). Geometry is also important for tissue durability, where the intrinsic asymmetry of the root prevents cusp deterioration by minimizing the transvalvular pressure and stress on the cusps (Dagum, Green et al. 1999). In addition to geometry, spatial and mechanical heterogeneity is also critical for function. During the majority of their in vivo strain range (<20%), valve leaflets are very extensible and compliant, which permits rapid and efficient opening (modulus ~54 kPa aortic leaflet radial direction and the pulmonary leaflets are less stiff (Mavrilas and Missirlis 1991; Christie and Barratt-Boyes 1995)). The sinus root wall however is significantly more rigid (aortic root modulus ~ 140-180 kPa and pulmonary root modulus ~50-85 kPa (Matthews, Azadani et al. 2010; Butcher, Mahler et al. 2011; Azadani, Chitsaz et al. 2012)), which helps maintain an open lumen under demanding hemodynamic loads (Sacks, Schoen et al. 2009). Tissue engineers have fabricated mechanically heterogeneous tissues, but specific benchmarks for valve engineering are unmet. An improved tissue engineering fabrication strategy should 1) effectively replicate native valve geometry and 2) effectively replicate regional mechanical heterogeneity.

Traditional *de novo* valve scaffold engineering involves manually shaping valve root and leaflet geometries out of polymer scaffold and seeding them with cells. A number of synthetic (poly-glycolic acid, polylactic acid, poly-4-hydroxybutyrate, polyhydroxyalkanoate) (Sodian, Hoerstrup et al. 2000; Sutherland, Perry et al. 2005; Balguid, Mol et al. 2009; Gottlieb, Kunal et al. 2010; Ramaswamy, Gottlieb et al. 2010; Sales, Mettler et al. 2010; Schmidt, Dijkman et al. 2010; Sodian, Schaefermeier et al. 2010; Eckert, Mikulis et al. 2011; van Geemen, Driessen-Mol et al. 2012) and biological polymeric (collagen I, fibrin) (Neidert and Tranquillo 2006; Robinson, Johnson et al. 2007; Flanagan, Sachweh et al. 2009) scaffolds have been created, mechanically conditioned *in vitro*, and tested in animal models. In the longest such trial to date (8 months within a growing sheep model), engineered valves (leaflet + conduit) were still functional but mildly stenotic, suggesting that the leaflets lacked sufficient compliance (Sutherland, Perry et al. 2005). While the exact cause is unknown, forming the root and leaflets with the same scaffold material mesh may have created root walls that are too compliant and/or cusps that are too stiff, both of which are characteristics of valve pathology (Butcher, Simmons et al. 2008). Incorporation of heterogeneity into tissue engineered valves with different root versus leaflet materials has been achieved, but this required the different parts to be fabricated sequentially and then joined with sutures manually (Shinoka, Ma et al. 1996; Sodian, Sperling et al. 1999).

Automated manufacturing technology has the potential to fabricate tissue-engineered scaffolds more rapidly with higher anatomical precision. Stereolithographic 3D printing and extrusion based 3D printing have both been used to fabricate scaffolds on the scale of heart valves. Schaefermeier et al. used stereolithography to fabricate a silicone aortic valve replica based on X-ray computed tomography (CT) scans and then used the replica to mold a PGA valve scaffold (Sodian, Loebe et al. 2002; Schaefermeier, Szymanski et al. 2009). Extrusion based 3D printing has been employed to engineer hard tissue scaffolds such as knee menisci and intervertebral disks complete with encapsulated cells (Cohen, Malone et al. 2006; Ballyns, Cohen et al. 2010). This process can rapidly recreate 3D computer aided design (CAD) models by slicing them into layers and building the layers upward using deposition tools that can extrude a wide range of materials. Adapting 3D printing technology to fabricate soft tissue heart valve scaffolds, however, requires overcoming the additional challenges of 1) adapting highly extensible elastomeric cell-friendly materials for 3D printing, and 2) printing complex soft tissues with overhanging structures and both internal and external geometric features.

Hydrogels can be designed to mimic mechanical and biological properties of soft tissue, and can be controlled for direct 3D printing. By modifying polymer precursors hydrogels can have tunable mechanics, provide attachment and signals to cells, have custom degradability, and be modified to allow for photo and chemical crosslinking (Benton, Fairbanks et al. 2009; Huebsch, Arany et al. 2010; Kloxin, Kloxin et al. 2010; Pedron, Kasko et al. 2010; Chandler, Berglund et al. 2011; Hutson, Nichol et al. 2011). The technology exists to rapidly 3D print clinically sized, geometrically complex constructs with hydrogels (Arcaute, Mann et al. 2006; Ballyns, Cohen et al. 2010; Fedorovich, Schuurman et al. 2012), but it has not been utilized for engineering heart valves. 3D printing clinically sized tissues (>10 mm) with high anatomical precision has been primarily demonstrated for hard tissues such as bone and cartilage (Hollister 2005; Ballyns, Cohen et al. 2010; Cipitria, Lange et al. 2012). Clinically sized soft tissues are a small minority of the 3D printing literature, dominated by vascular conduits and networks that don't exhibit external geometric complexity or non-self-supporting geometries (Skardal, Zhang et al. 2010; Xu, Chai et al. 2012). Micro-scale 3D printed tissues have been fabricated with very fine precision using hydrogels, but have been limited to tissues ~5 mm tall or less (Liu and Bhatia 2002; Chan, Zorlutuna et al. 2010; Gauvin, Chen et al. 2012). This leads us to investigate utility of extrusion based 3D hydrogel printing for enabling rapid soft tissue hydrogel fabrication at clinically necessary sizes (>10 mm) with high spatial precision.

In this study, we implemented an on-board photocrosslinking system to enable simultaneous 3D extrusion printing and curing of hydrogels in complex aortic valve geometries. We additionally compare 3D printed geometry accuracy for native and axisymmetric valve anatomy using micro-CT. Cell viability and spreading of PAVIC cultured on 3D printed scaffolds were assessed over 21 days.

2. Materials and Methods

2.1. Base hydrogel formulation

Poly(ethylene glycol)-diacrylate (PEG-DA) was used as the base polymer precursor for this study. Many tissue engineering applications have used PEG-DA as a scaffold component tbecause it is a biocompatible, photocrosslinkable elastomer whose mechanical properties can be easily modified (Peyton, Raub et al. 2006; Guo and Chu 2007). 700 and 8000MW PEG-DA precursors were chosen for this study because their differences in molecular weight have been shown by others to correlate with hydrogel stiffness (Hahn, McHale et al. 2007; Huebsch, Arany et al. 2010; Browning, Wilems et al. 2011; Hutson, Nichol et al. 2011). PEG-DA undergoes slow hydrolytic degradation in vivo, and it can also be functionalized and combined with other precursors to encourage cell attachment (Peyton, Raub et al. 2006; Hutson, Nichol et al. 2011; Browning and Cosgriff-Hernandez 2012). Several studies employing stereolithography printing have demonstrated that photopolymerizing layered hydrogels using ultraviolet (UV) irradiation can yield 3D structures (Dhariwala, Hunt et al. 2004; Arcaute, Mann et al. 2006; Chan, Zorlutuna et al. 2010). These features support the use of PEG-DA as base polymer precursor for 3D printing of valve scaffolds.

The base hydrogel solution used in this study consisted of phosphate buffered saline (PBS), photoinitiator, and PEG-DA. Photoinitiator (Irgacure 2959; Ciba Specialty Chemicals, Tarrytown, NJ) was first dissolved in PBS at 60°C. After cooling the solution to room temperature, 700 MW (Sigma Aldrich, St. Louis, MO) and/or 8000 MW PEG-DA (synthesized by the authors (Guo and Chu 2005)) were dissolved into the solution.

2.2. Mechanical testing of base hydrogel blends

We examined the degree of biomechanical tunability in PEG-DA hydrogels by performing uniaxial ring tensile tests (Seliktar, Black et al. 2000; Seliktar, Nerem et al. 2001). Hydrogel precursor solutions were prepared by dissolving 0.1-0.2% w/v photoinitiator and 0-20:0-10% 700:8000 MW PEG-DA in PBS, where amount of photoinitiator was directly proportional to increasing PEG-DA concentration (to maintain 1% w/w precursor to polymer). For the extremes, 10% w/v 8000 MW and 20% w/v 700 MW PEG-DA hydrogels were optimal for handling (room temperature solubility and resulting robust gels). Precursor solutions were crosslinked at 365 nm UV light at 245 mW/cm^2 inside 4-well plates for 10 minutes (EN280L lamp; Spectroline, Westbury, NY). Rings were created from crosslinked hydrogel cylinders with an 8-mm biopsy punch and then secured in a vertical orientation between two hook fixtures within a PBS bath on the testing platform (EnduraTec 3200; Bose Electroforce, Eden Prairie, MN). Samples were loaded quasi-statically at 0.02mm/sec until failure (strain rate is 0.005/sec).

2.3. 3D printing system and hydrogel modification

Detailed specifications and mechanics of the open-source Fab@Home™ Model 1 extrusion based 3D printing (robocasting) can be found at www.fabathome.org and in our previous studies (Cohen, Malone et al. 2006; Malone and Lipson 2007). For this study, the printing platform was modified to carry three syringes. In addition, we built a UV-LED crosslinking module, in which four LEDs were arranged in a 2×2 formation and mounted directly on the syringe carriage (crosslinking energy at the printing surface was 16.5 mW/cm^2/LED, (Nichia America Corporation, Wixom, MI) (figure 1(a)). For sterile printing, an autoclavable bag attached with a UV transparent film with access ports for the nozzles was autoclaved. The bag was then mounted below the syringe carriage inside a laminar hood, and the precursor solutions were printed through the access ports while the UV-LED crosslinked the printed solutions through the film.

Un-modified soluble alginate (LF10/60, FMC BioPolymer, Drammen, Norway) was mixed into PEG-DA precursor formulations to temporarily increase viscosity during the printing extrusion process. While 2% w/v alginate mixed in PBS is sufficiently viscous to be extrudable (Cohen, Malone et al. 2006), pilot studies found that PEG-DA dramatically increased the solubility of alginate. We found adding 10-15% w/v alginate to a PEG-DA solution achieves suitable extrusion viscosity. In addition, PEG-DA extrusion was sensitive to the salt concentration of the buffer in a MW dependent manner. Precursor solutions made with 1x PBS and only 700 MW PEG-DA could not be printed due to phase separation, but this was overcome by changing the salt concentration (13.7 mM NaCl) but maintaining normal pH.

2.4. Measuring crosslinking time of hydrogels

The crosslinking time required of the printed precursor solutions need to match each other in order to fabricate heterogeneous hydrogel layers. Therefore, we investigated how crosslinking time was controlled by molecular weight PEG-DA and varying photoinitiator concentration. Hydrogel precursor solution containing 10-15% w/v alginate and 0.2-2.0% w/v Irgacure was first injected into 4-8 mm diameter, 1-mm thick disc molds made with either 700 MW or 8000 MW PEG-DA. The solutions were then exposed to 365 nm UV light from the crosslinking module. Minimum crosslinking time was defined as the point when the hydrogel gel transitioned from liquid to solid. This was the point where the hydrogel disc did not flow after the mold was removed, did not flow in response to gentle compression with a spatula, and held its shape upon being transferred into PBS (did not dissolve).

2.5. Valve geometry design

Two aortic valve models were created for printing. The first model, an axi-symmetric aortic valve geometry including the sinus and leaflets (kind gift of Dr. Reetu Sing), was generated in SolidWorks (Waltham, MA) as shown in figure 1(b). For the second model, a porcine aortic valve conduit obtained fresh at slaughter (Shirk Meats, Himrod, NY) was fixed in formalin (figure 1(c)) and scanned with the leaflets in a partially open position via micro-CT at 100 μm voxel size, 80 keV, 30 mA, 800 angles, 30 ms exposure time, 30 gain, and 20 offset (eXplore CT120; GE Healthcare, United Kingdom). The root and leaflet regions in the resulting DICOM scans were segmented via intensity thresholds (figure 1(d)) and rendered into 3D geometries in stereolithography format of Standard Tessellated Language (STL) files (Mimics 12.0; Materialise, Leuven, Belgium) (figure 1(e)). A separate temporary scaffold to support the ostia lumens was generated by Boolean subtraction.

2.6. Heterogeneous valve printing

Based on the mechanical testing crosslinking test results (figure 2), we established a biomechanically stiff PEG-DA formulation (20%:0% 700:8000 MW) to comprise the aortic root wall and a compliant and extensible hydrogel for the leaflets formulation (5%:7.5% 700:8000 MW). Using these ratios, stiff hydrogel (13.7 mM NaCl, 1% w/v photoinitiator, 20:0% PEG-DA, 12.5% w/v alginate) and compliant hydrogel (PBS, 1% w/v photoinitiator, 5:7.5% w/v PEG-DA, 15.0% w/v alginate) precursor solutions were prepared. 1% photoinitiator concentration was chosen since it enabled both hydrogel formulations to crosslink rapidly in about 30-60 seconds, which was comparable to the print time of each layer.

Precursor solutions were loaded into the deposition syringes fitted with 0.83 mm inner diameter nozzles. After importing the STL geometries, the software generated print paths at 0.6-0.7 mm pathheight and 0.8-0.9 mm pathwidth (figure 1(f)) for all geometries. The aortic root was printed with the stiff hydrogel while the leaflet was printed with the compliant PEG-DA hydrogel at 0.6 and 0.4 mL/min and traversing rate of 6 and 3 mm/s, respectively. The UV crosslinking array attached on the carriage crosslinked the printed hydrogel paths as they were extruded at 16.5 mW/cm^2 during fabrication (figure 2(e)). To print the support geometry for the overhanging ostia and leaflets, a third syringe was loaded with a non-photocrosslinking alginate-gelatin solution. The temporary support structure printed with this formulation was able to support itself without crosslinking due to the high viscosity of the solution, but was easily removed by rinsing in aqueous buffer. To assess size dependent accuracy and scalability, valve scaffolds were printed at 100, 50, and 18% of the original model volume.

2.7. Shape fidelity evaluation of aortic valve scaffolds

Shape fidelity was assessed quantitatively using micro-CT. Valve conduits were printed using 20% w/v 700 MW PEG-DA hydrogel (13.7 mM NaCl, 1% w/v photoinitiator, 12.5% w/v alginate). Conduits were scanned directly after printing via micro-CT. To test how swelling affects geometry, they were also hydrated in PBS overnight and scanned. Resulting scans were then reconstructed into STL geometries using MicroView (GE Healthcare). Surface deviations between printed and native STL models were quantified through autoregistration and heat maps in Geomagics Qualify (v9.0; Research Triangle, NC) (Ballyns, Cohen et al. 2010). We chose ±10% in diameter as the tolerance threshold for valve fabrication since greater than 10% diameter mismatch in non-living prosthetic valves has been shown to impair hemodynamic function (Pibarot and Dumesnil 2006).

Assessing the internal geometric fidelity was impossible with surface heat maps. Therefore, slice-by-slice comparison of each printed layer was also performed. Micro-CT generated

virtual slices of the printed scaffolds were compared to the corresponding image-derived layers of the original valve STL files in the XY-plane (figure 2(d)). The two slices were overlapped and compared using Boolean operations. For a given slice, regions printed outside the target print area were designated overprint error, and regions that were not printed within the target area were designated underprint error.

2.8. Cell viability and spreading

Porcine aortic valve interstitial cells (PAVIC) were employed as model cell source to investigate valve scaffold biocompatibility because VIC are the main cell type that populates valve leaflets (Butcher, Simmons et al. 2008). PAVIC were isolated via collagenase digestion as previously described (Butcher, Penrod et al. 2004) and cultured with Dulbecco's Modified Eagle's Medium (DMEM; Invitrogen, Carlsbad, CA) supplemented with 10% fetal bovine serum (FBS; Invitrogen) and 1% penicillin/streptomycin (PS; Invitrogen). Cells were used at passage 5-8.

Sterile 12 mm diameter aortic valve conduits were printed with 700 MW PEG-DA hydrogel. Conduits were rinsed in PBS overnight to leach out the non-crosslinking alginate. They were then transferred to a 50 mL conical vial containing 20×10^6 PAVIC in 40 mL of culture media. After 24 hours of rotary seeding at 37°C, 5% CO_2 (day 1), valve conduits were cultured in flasks for 7 and 21 days. Media was exchanged every 48 hrs. Conduits were then stained with 4 mM calcein-AM and 2 mM ethidium homodimer (LIVE-DEAD, Invitrogen) for 30 min at 37°C and then rinsed with PBS. Conduits were cut with a razor blade and imaged using an epiflourescence stereomicroscope (SteREO Discovery.V20; Zeiss, Germany).

Since PEG-DA is virtually non-adhesive and non-adsorptive in its unmodified form (Hutson, Nichol et al. 2011), we tested whether collagen fibrillized within the PEG-DA hydrogels could provide enhanced cell activity. Collagen I was extracted from rat tail tendons (Pel-Freez Biologicals, Rogers, AR) and dissolved in sterile 0.1% acetic acid for 24 hrs prior to hydrogel preparation as previously described (Bowles, Williams et al. 2010). Low concentrations of collagen (0.1 or 0.5 mg/mL) were mixed in 3x DMEM containing 10% FBS, and 0.1M NaOH was added to neutralize pH. This solution and PEG-DA hydrogel precursor solutions were kept on ice until they were combined. The combined solution was photocrosslinked in disc molds and then incubated at 37°C for 30 minutes to allow the collagen monomers to fibrillize. Ultrastructure of completely crosslinked PEG-DA hydrogels with and without collagen and/or alginate leaching prior to seeding was analyzed via scanning electron microscopy (SEM). Fully hydrated hydrogels were flash frozen, lyophilized, mounted on aluminum SEM stubs, and imaged (Leo 1550 FESEM Cornell Center for Materials Research, Ithaca, NY) (Benton, DeForest et al. 2009). Image J was used to analyze mean pore area for each representative image. Hydrogel discs were then rinsed and surface-seeded with 0.5×10^6 PAVIC/mL. Cell circularity (index of cell spreading) was quantified using ImageJ.

2.9. Statistical analysis

Mechanical testing was conducted with $n = 3$ rings per formulation. Crosslinking tests were conducted with $n \geq 5$ disks per condition. Fidelity and viability assessment was performed with $n = 3$-4 printed valve scaffolds. Measurements were indicated as mean and standard deviation unless noted otherwise. Statistical comparisons were made using 1-way ANOVA followed by Tukey modified t-tests. $P<0.05$ denoted significance. For SEM pore area analysis statistical comparisons were made using 2-way ANOVA with Tukey Post-test, $p < 0.05$. 2-way factors are gel MW and treatment (unrinsed, rinsed, collagen).

3. Results

3.1. Mechanical properties of hydrogels

Mixing of 700 and 8000 MW PEG-DA resulted in elastomeric hydrogels with a broad range of mechanical properties. In general, hydrogels became stiffer and less extensible as the proportion of 700 MW PEG-DA increased (figure 2(a, b)). 0:10% w/v (700:8000 MW) hydrogels exhibited very extensible, nearly linear elastic behavior with modulus of 5.3 ± 0.9 kPa through a strain of 1.6 ± 0.1. 20:0% w/v hydrogels, on the other hand, exhibited nonlinear tensile stress-strain behavior, with an approximately 13-fold greater modulus at 74.6 ± 1.5 kPa through a strain of 0.50 ± 0.15. Intermediate ratios between these extremes created stress-strain responses between the individual polymer extremes (figure 2(a)). As examples, 5:7.5% w/v hydrogels exhibited modulus of 12.7 ± 1.6 kPa though a strain of 2.0 ± 0.5, and 15:2.5% w/v hydrogels exhibited modulus of 42.5 ± 1.0 kPa through a strain of 0.94 ± 0.01. Modulus between 5:7.5% and 0:10% w/v did not vary significantly. Collectively, these results show that PEG-DA hydrogels exhibit nonlinear elastic mechanics that can be tuned through polymer mass and molecular weight ratio.

3.2. Effect of photoinitiator concentration on hydrogel crosslinking time

PEG-DA hydrogel crosslinking time decreased exponentially with increasing concentrations of Irgacure (figure 2(c)). 700 MW PEG-DA hydrogels crosslinked 5-10 fold faster than 8000 MW hydrogels at the same Irgacure concentration, likely because of the increased availability of polymer chains and active end groups. At 0.2% w/v Irgacure, 700 MW hydrogels crosslinked in 98 ± 3 s, but 8000 MW hydrogels crosslinked at 1140 ± 60 s. At 2% w/v Irgacure, 700 MW hydrogels took only 17 ± 1 s to crosslink, and 8000MW hydrogels took just 78 ± 8 s. These results demonstrate that hydrogel crosslinking time can be tuned with photoinitiator concentration, and they further suggest that balancing photoinitiator concentration for each base material can maintain overall crosslinking kinetics.

3.3. Rapid printing of heterogeneous and scaled valve scaffolds

Crosslinking the hydrogel during fabrication enabled the two different hydrogels formulations to fuse and integrate with each other and between printed layers. Printed valve conduits retained biomechanical heterogeneity, where the leaflets extended and bent easily while the root remained relatively rigid (figure 3(b, e). Both anatomic and axially symmetric valve scaffolds were successfully printed at 100%, 50%, and 18% of the original model volume. The valve conduits had inner diameters (ID) of 22, 17, and 12 mm (figure 3(c, f)) and heights of 25, 20, and 14 mm, respectively. Gross anatomical features such as ostia, commissures, and sinuses were present at all sizes. The 12 mm ID valve conduits were fabricated in 14 minutes, the 17 mm in 30 minutes, and the 22 mm in 45 minutes. Together, these results support that 3D printing strategy can rapidly generate mechanically heterogeneous, anatomically complex valve conduits.

3.4. Shape fidelity

We further characterized their shape fidelity using surface deviation analysis through micro-CT imaging. For the 22, 17, and 12 mm ID image-derived, hydrated valve scaffolds, 93.3 ± 2.6, 85.1 ± 2.0, and 73.3 ± 5.2% of the points laid within the ±10% diameter threshold respectively (figure 4(a, c)). For the axial symmetric hydrated valve scaffolds, 89.1 ± 4.0, 84.1 ± 5.6, and 66.6 ± 5.2% of the points were within ±10% threshold (figure 4(b, c)). These results indicate that the 3D printing strategy generates scaffolds with high geometric precision, but accuracy decreased somewhat with reduced size. For the image-derived valve scaffolds, overprint error (points lying beyond +10% threshold) predominated the underprint

error (points beyond −10% threshold) (error proportion over:under was 89.0:11.0%, 90.0:10.0%, and 82.3:17.7%, for 22, 17, and 12 mm ID, respectively) throughout the root and leaflet (figure 4(d) solid bars). Overprint error also predominated over the underprint error in the axially symmetric valve scaffolds (88.2:11.8, 92.7:7.3, and 94.4:5.6%, for 22, 17, and 12 mm ID in over:under ratio, respectively) (figure 4(d) striped bars).

Slice-by-slice analysis to assess the internal geometic fidelity indicated that overlapping area percentage decreased as the size of the image-derived valve scaffolds decreased (81.7 ± 1.9 to 61.9 ± 4.3% from 22 to 12 mm ID) (figure 5(a)). Total overprint and underprint area percentage between fully hydrated and scaffolds scanned immediately after printing was not significantly different, but the error locations were different. Non-hydrated scaffolds contained overprinted regions on the inner walls, but hydrated valve scaffolds were underprinted on the inner walls and overprinted on the outer walls (figure 5(b)). These results suggest that residual error in final shape is caused in part by outward but not inward swelling.

3.5 Alginate removal and cell cytocompatibility of hydrogel scaffolds

PEG-DA hydrogel structure appears to be modulated by molecular weight and type of additives (alginate and collagen I) (figure 6). The SEM images show that PEG-DA precursor solution + 10% w/v alginate appears to form small pores, with alginate packing the structure (figure 6 (a, b)). Alginate leached out of hydrogels rinsed in an aqueous buffer (nearly 100% within 24 hours according to weight), and this was confirmed with the SEM images where PEG-DA pore size appears to increase for 700 and 8000 MW, respectively (figure 6 (c, d)). We noticed that post-polymerization the alginate hydrogels were opaque and were opaque even after leaching, which suggests that a microscopic amount of alginate may persist. When PEG-DA precursor solutions with alginate were further mixed with neutralized collagen I before crosslinking (0.01% w/v collagen in total solution) and then alginate was leached out, the structures appeared more fibrous (figure 6 (e, f)). Image analysis of mean pore area for each representative SEM image a) 6.1±1.0 um^2 , b) 14.0±2.8 um^2, c) 36.6±7.4 um^2, d) 103.5±14.1 um^2, e) 103.1 ± 21.3 um^2, and f) 154.8± 36 um^2. The pore size was non-uniform.. Pores in a, b, c were significantly different from d, e, f.

PAVIC seeded valve scaffolds contained cells across the entire surface of the conduits, and to a lesser degree within the root and leaflet interstitium (figure 7 (a, b)). Cells were 91.3 ± 10.7% viable at day 1. At day 7 and 21 cells were 100% viable. For PAVIC cultured on disks, cell morphology was tested on the base hydrogel formulation and with 0.1 or 0.5 mg/ml collagen I to the precursor solution (figure 8). The mean circularity of PAVIC on 700 MW PEG-DA base gels decreased significantly over time (0.83 ± 0.03 to 0.74 ± 0.01 between day 1 and 21) (figure 8(a)). Meanwhile, PAVIC circularity in 8000 MW PEG-DA hydrogels did not change significantly over time (0.80 ± 0.01, 0.80 ± 0.01, and 0.79 ± 0.02 at day 1, 7, and 21, respectively) (figure 8(b)). Circularity after addition of 0.1 or 0.5 mg/mL of type I collagen into either PEG-DA hydrogel did not change over time. These results indicated that PAVIC adhere and spread on the PEG-DA hydrogel (with alginate removed) scaffold material, but that the addition of collagen at 0.1 or 0.5 mg/mL did not improve cell spreading.

4. Discussion

Replicating mechanical heterogeneity and geometry of the native tissue has been increasingly considered critical for engineering living *de novo* aortic heart valves. We developed and implemented a 3D printing strategy combining on-board UV photocrosslinking with mechanically tunable PEG-DA hydrogels to rapidly fabricate anatomically complex, mechanically heterogeneous valve scaffolds at different sizes. These

scaffolds can be seeded with valve cells, which populated the surface and reached the interstitium and remained viable to at least 21 days. The relatively rapid printing times (14-45 minutes), with no requirement for further processing post-fabrication (e.g. joining components), support that 3D printing is an efficient process for engineering anatomically precise soft tissue scaffolds.

Matching patient-specific size is integral for proper valve function. An ongoing limitation of current valve prosthetics is that the prosthetics are often too big for pediatric and young patients. The smallest manufactured mechanical valve to date spans 17 mm (St. Jude Medical Mechanical Heart Valve; St. Jude Medical Inc., Minneapolis, MN). Smaller sized mechanical prosthetic valves have higher gradients and are effectively occluded more by the mechanical leaflets that lie in the flow field (Dasi, Simon et al. 2009). We were able to print valve conduit scaffolds spanning a range of clinically relevant sizes as small as 12 mm ID, which is approximately the size of a 6 month infant aortic valve, and up to 22 mm ID valve, which is an adult size. We also demonstrated that multiple geometries, a simplified axial symmetric geometry and a medical imaging derived geometry, can be printed using this printing technique. The capability to incorporate direct sizing and patient derived geometry into valve scaffolds suggests that 3D printing could potentially alleviate the prosthetic sizing concern. It is important to note that this study focused on valve scaffold fabrication, and determination of function will require *in vitro* flow studies that are beyond the scope of this work.

Assessing shape fidelity is important for tissue engineering. The common approach of visual inspection, mainly by identifying the presence of key features such as the coronary ostia and the sinuses (Sodian, Loebe et al. 2002), is helpful as a cursory screening process. However, it cannot pinpoint deviations or tolerances of scaffolds in detail required for scale-up manufacturing or complex patient specific applications. Calipers provide limited information on how to improve shape fidelity (Ballyns, Gleghorn et al. 2008), particularly for a complex shape such as a valve where leaflet and root tissue thickness may vary along their lengths. In this study, we used an image-based method to quantitatively assess print accuracy, which was as high as 93% that reduced somewhat as the inner diameter size decreased. This evaluation, which supplemented the visual inspections, provided a more comprehensive demonstration that the printed scaffolds exhibit geometric fidelity.

Our shape fidelity analysis suggested steps that can be taken to improve print accuracy. The same print parameters that yielded high fidelity for 22 mm ID valves produced much more overprint for 12 mm ID valves, suggesting that the print paths were too wide for filling in smaller regions of the 12 mm ID valves without overprinting. Therefore, employing smaller extrusion rate and narrower nozzle diameters (to increase print resolution) would be a scaled approach for optimizing the printing. This adjustment would have to be balanced with an accompanying increase in print time, but the time would still likely remain to be less than 45 minutes, which was the print time for the 22 mm ID valve. The other step is to adjust for swelling. Compensating for swelling is important because hydrogels have characteristic equilibrium swelling ratio (Bryant and Anseth 2002; Ma and Elisseeff 2005). Since our scaffolds expanded outward but not inward, we suspect that surface tension on the inner walls prevented the scaffolds from swelling inward. Hydrogel scaffolds should therefore be printed thinner than the target size so that the expanded final state matches the native model. By analyzing the fidelity of the printing process layer by layer, we were also able to pinpoint anatomical features that were locally over- or underprinted. Therefore, the fidelity of the final printed shape can likely be improved by adjusting the initial print paths for each layer, but the specific changes will be dependent on the relative thicknesses of each polymer component, the curvature of the shape, and the kinetics of the extrusion process.

Ultimately, tissue engineered heart valve scaffolds must be able to support cell adhesion and migration. The 3D printed scaffolds were populated at the surface and with high viability, indicating that the printing method and resulting material were not cytotoxic. Seeded scaffolds and disks were fed and rinsed with media every 48 hours, and it is possible that cells unable to attach or dying washed away from the valve scaffolds over time. We expect that cell viability is conservatively maintained at the same levels as day 1. We measured a circularity of 0.7-0.8 for all conditions, which indicates that cells were in an elliptically spread configuration. Contrary to our expectations, the addition of collagen into the PEG-DA hydrogels did not promote further spreading. While our SEM images show a hydrogel structure that appears more fibrous upon the addition of collagen to the precursor solution, this addition did not significantly affect the cell behavior. What is interesting to note is that other studies indicate that PEG-DA is non-adsorptive (Rogers, Pagaduan et al. 2011) and alginate is non-absorptive due to electrostatic repulsion (Rowley, Madlambayan et al. 1999). Additionally, alginate does not have groups that provide any means for mammalian cell attachment (Genes, Rowley et al. 2004), and PEG-DA alone is also reported to discourage cell attachment (Hutson, Nichol et al. 2011). We hypothesize that that a small amount of alginate must remain in the PEG-DA network and the combination roughens the scaffold surface to permit cell adhesion, similar to the microphase separation that is seen in multicomponent PEG-DA hydrogels (Zhang, Wang et al. 2011).

Controlling the mechanical heterogeneity between the root and leaflet has been a major focus in engineering valve scaffolds for ensuring proper hemodynamics and durability. We believe 3D printing can be advantageous for incorporating heterogeneity since it can establish relative differences between tissue regions using these synthetic materials with ease. The ability to rapidly fabricate scaffolds also provides a platform for studying how cells behave on heterogeneous environments, which is crucial to investigate since the modulus of the scaffold material can direct cell migration (Tayalia, Mendonca et al. 2008), spreading (Kloxin, Kloxin et al. 2010), and differentiation (Engler, Sen et al. 2006; Kloxin, Kloxin et al. 2010). The modulus numbers in this study fall within the range of values demonstrated by other studies investigating the tunability of PEG-DA hydrogel tensile mechanical properties (Hahn, McHale et al. 2007; Hou, Schoener et al. 2010; Browning, Wilems et al. 2011). Our results overall suggest that PEG-DA hydrogels can partially recreate the mechanical properties of the aortic valve and pulmonary valve. At physiological tensile strains (0.01-0.20) and low strain rates, the moduli of PEG-DA hydrogels tested here (700 MW: ~75 kPa; 8000 MW: ~5 kPa) fall within range of modulus of native leaflet tissue in the radial direction (~54 kPa (Mavrilas and Missirlis 1991)). However, they are softer than the aortic valve sinus tissue (~ 140-180 kPa (Matthews, Azadani et al. 2010; Butcher, Mahler et al. 2011; Azadani, Chitsaz et al. 2012)). The mechanical properties of the PEG-DA hydrogels more closely match pulmonary valve sinus tissue (~50-85 kPa) (Matthews, Azadani et al. 2010). With the clinical success of the Ross procedure, the pulmonary valve has been identified as a first target for tissue engineered heart valves (Butcher, Mahler et al. 2011), and duplicating those mechanics may be initially more relevant to the field. Additionally, it has been shown that cellularized PEG-DA hydrogels with the addition of moieties that allow for remodeling have improved mechanical properties with dynamic culture (Hahn, McHale et al. 2007). Therefore, this fabrication strategy for engineering valve conduits could be pursued further with the addition of a variety of moieties to PEG-DA hydrogels and dynamic conditioning.

5. Conclusions

This study demonstrated that 3D printing and photocrosslinking hydrogels can rapidly fabricate anatomical scaffolds exhibiting mechanical heterogeneity and cytocompatibility. This manufacturing process was demonstrated with PEG-DA, but we believe this method

could be adapted for use with other photocrosslinkable polymers. Further work is necessary to complete the translation of this strategy to the clinic. Continued effort must be made to understanding how cells on constructs would remodel the scaffold in simulated hemodynamic conditions. Further investigation of multiple polymer blends to be incorporated into heterogeneous valve conduits would also be required to mimic the complete low and high magnitude strain behaviors of native valve tissues. Our findings herein are encouraging steps toward improved valve scaffold designs for both adult and pediatric valve disease.

Acknowledgments

We thank Mark Riccio, Dr. Jeffrey Ballyns, Philip Buskhol, Dr. Claudia Fischbach, and Dr. Michael Schuler for their technical assistance. This research was supported by the Morgan Family Foundation, The Hartwell Foundation, the National Science Foundation (CBET-0955172), NSF Graduate Research Fellowship, and the American Heart Association (AH0830384N). The authors have no financial disclosures.

References

Arcaute K, Mann BK, et al. Stereolithography of three-dimensional bioactive poly(ethylene glycol) constructs with encapsulated cells. Ann Biomed Eng. 2006; 34(9):1429–1441. [PubMed: 16897421]

Azadani AN, Chitsaz S, et al. Biomechanical comparison of human pulmonary and aortic roots. Eur J Cardiothorac Surg. 2012

Balguid A, Mol A, et al. Hypoxia induces near-native mechanical properties in engineered heart valve tissue. Circulation. 2009; 119(2):290–297. [PubMed: 19118259]

Ballyns JJ, Cohen DL, et al. An optical method for evaluation of geometric fidelity for anatomically shaped tissue-engineered constructs. Tissue Eng Part C. 2010; 16(4):693–703.

Ballyns JJ, Cohen DL, et al. An optical method for evaluation of geometric fidelity for anatomically shaped tissue-engineered constructs. Tissue Eng Part C Methods. 2010; 16(4):693–703. [PubMed: 19788346]

Ballyns JJ, Gleghorn JP, et al. Image-guided tissue engineering of anatomically shaped implants via MRI and micro-CT using injection molding. Tissue Eng Part A. 2008; 14(7):1195–1202. [PubMed: 18593357]

Bellhouse BJ, Bellhouse FH, et al. Fluid mechanics of the aortic root with application to coronary flow. Nature. 1968; 219(5158):1059–1061. [PubMed: 5673366]

Benton JA, DeForest CA, et al. Photocrosslinking of gelatin macromers to synthesize porous hydrogels that promote valvular interstitial cell function. Tissue Eng Part A. 2009; 15(11):3221–3230. [PubMed: 19374488]

Benton JA, Fairbanks BD, et al. Characterization of valvular interstitial cell function in three dimensional matrix metalloproteinase degradable PEG hydrogels. Biomaterials. 2009; 30(34):6593–6603. [PubMed: 19747725]

Bowles RD, Williams RM, et al. Self-assembly of aligned tissue-engineered annulus fibrosus and intervertebral disc composite via collagen gel contraction. Tissue Eng Part A. 2010; 16(4):1339–1348. [PubMed: 19905878]

Browning MB, Cosgriff-Hernandez E. Development of a biostable replacement for PEGDA hydrogels. Biomacromolecules. 2012; 13(3):779–786. [PubMed: 22324325]

Browning MB, Wilems T, et al. Compositional control of poly(ethylene glycol) hydrogel modulus independent of mesh size. J Biomed Mater Res A. 2011; 98(2):268–273. [PubMed: 21626658]

Bryant SJ, Anseth KS. Hydrogel properties influence ECM production by chondrocytes photoencapsulated in poly(ethylene glycol) hydrogels. J Biomed Mater Res. 2002; 59(1):63–72. [PubMed: 11745538]

Butcher JT, Mahler GJ, et al. Aortic valve disease and treatment: the need for naturally engineered solutions. Adv Drug Deliv Rev. 2011; 63(4-5):242–268. [PubMed: 21281685]

Butcher JT, Penrod AM, et al. Unique morphology and focal adhesion development of valvular endothelial cells in static and fluid flow environments. Arterioscler Thromb Vasc Biol. 2004; 24(8):1429–1434. [PubMed: 15117733]

Butcher JT, Simmons CA, et al. Mechanobiology of the aortic heart valve. J Heart Valve Dis. 2008; 17(1):62–73. [PubMed: 18365571]

Chan V, Zorlutuna P, et al. Three-dimensional photopatterning of hydrogels using stereolithography for long-term cell encapsulation. Lab Chip. 2010; 10(16):2062–2070. [PubMed: 20603661]

Chandler EM, Berglund CM, et al. Stiffness of photocrosslinked RGD-alginate gels regulates adipose progenitor cell behavior. Biotechnol Bioeng. 2011; 108(7):1683–1692. [PubMed: 21328324]

Christie GW, Barratt-Boyes BG. Mechanical properties of porcine pulmonary valve leaflets: how do they differ from aortic leaflets? Ann Thorac Surg. 1995; 60(2 Suppl):S195–199. [PubMed: 7646158]

Cipitria A, Lange C, et al. Porous scaffold architecture guides tissue formation. J Bone Miner Res. 2012; 27(6):1275–1288. [PubMed: 22407823]

Cohen DL, Malone E, et al. Direct freeform fabrication of seeded hydrogels in arbitrary geometries. Tissue Eng. 2006; 12(5):1325–1335. [PubMed: 16771645]

Dagum P, Green GR, et al. Deformational dynamics of the aortic root: modes and physiologic determinants. Circulation. 1999; 100(19 Suppl):II54–62. [PubMed: 10567279]

Dasi LP, Simon HA, et al. Fluid mechanics of artificial heart valves. Clin Exp Pharmacol Physiol. 2009; 36(2):225–237. [PubMed: 19220329]

Dhariwala B, Hunt E, et al. Rapid prototyping of tissue-engineering constructs, using photopolymerizable hydrogels and stereolithography. Tissue Eng. 2004; 10(9-10):1316–1322. [PubMed: 15588392]

Eckert CE, Mikulis BT, et al. Three-dimensional quantitative micromorphology of pre- and post-implanted engineered heart valve tissues. Ann Biomed Eng. 2011; 39(1):205–222. [PubMed: 20853027]

Engler AJ, Sen S, et al. Matrix elasticity directs stem cell lineage specification. Cell. 2006; 126(4): 677–689. [PubMed: 16923388]

Fedorovich NE, Schuurman W, et al. Biofabrication of osteochondral tissue equivalents by printing topologically defined, cell-laden hydrogel scaffolds. Tissue Eng Part C Methods. 2012; 18(1):33–44. [PubMed: 21854293]

Flanagan TC, Sachweh JS, et al. In vivo remodeling and structural characterization of fibrin-based tissue-engineered heart valves in the adult sheep model. Tissue Eng Part A. 2009; 15(10):2965–2976. [PubMed: 19320544]

Gauvin R, Chen YC, et al. Microfabrication of complex porous tissue engineering scaffolds using 3D projection stereolithography. Biomaterials. 2012; 33(15):3824–3834. [PubMed: 22365811]

Genes NG, Rowley JA, et al. Effect of substrate mechanics on chondrocyte adhesion to modified alginate surfaces. Arch Biochem Biophys. 2004; 422(2):161–167. [PubMed: 14759603]

Gottlieb D, Kunal T, et al. In vivo monitoring of function of autologous engineered pulmonary valve. J Thorac Cardiovasc Surg. 2010; 139(3):723–731. [PubMed: 20176213]

Guo K, Chu CC. Synthesis and characterization of novel biodegradable unsaturated poly(ester amide)/poly(ethylene glycol) diacrylate hydrogels. Journal of Polymer Science Part A: Polymer Chemistry. 2005; 43(17):3932–3944.

Guo K, Chu CC. Controlled release of paclitaxel from biodegradable unsaturated poly(ester amide)s/poly(ethylene glycol) diacrylate hydrogels. J Biomater Sci Polym Ed. 2007; 18(5):489–504. [PubMed: 17550654]

Hahn MS, McHale MK, et al. Physiologic pulsatile flow bioreactor conditioning of poly(ethylene glycol)-based tissue engineered vascular grafts. Ann Biomed Eng. 2007; 35(2):190–200. [PubMed: 17180465]

Hoffman JI, Kaplan S. The incidence of congenital heart disease. J Am Coll Cardiol. 2002; 39(12): 1890–1900. [PubMed: 12084585]

Hollister SJ. Porous scaffold design for tissue engineering. Nat Mater. 2005; 4(7):518–524. [PubMed: 16003400]

Hou Y, Schoener CA, et al. Photo-cross-linked PDMSstar-PEG hydrogels: synthesis, characterization, and potential application for tissue engineering scaffolds. Biomacromolecules. 2010; 11(3):648–656. [PubMed: 20146518]

Huebsch N, Arany PR, et al. Harnessing traction-mediated manipulation of the cell/matrix interface to control stem-cell fate. Nat Mater. 2010; 9(6):518–526. [PubMed: 20418863]

Hutson CB, Nichol JW, et al. Synthesis and characterization of tunable poly(ethylene glycol): gelatin methacrylate composite hydrogels. Tissue Eng Part A. 2011; 17(13-14):1713–1723. [PubMed: 21306293]

Kloxin AM, Kloxin CJ, et al. Mechanical properties of cellularly responsive hydrogels and their experimental determination. Adv Mater. 2010; 22(31):3484–3494. [PubMed: 20473984]

Liu VA, Bhatia SN. Three-Dimensional Photopatterning of Hydrogels Containing Living Cells. Biomedical Microdevices. 2002; 4(4):257–266.

Ma, PX.; Elisseeff, JH. Scaffolding in tissue engineering. Taylor&Francis; Boca Raton: 2005.

Malone E, Lipson H. Fab@Home: The Personal Desktop Fabricator Kit. Rapid Prototyping J. 2007; 13:244–255.

Matthews PB, Azadani AN, et al. Comparison of porcine pulmonary and aortic root material properties. Ann Thorac Surg. 2010; 89(6):1981–1988. [PubMed: 20494060]

Mavrilas D, Missirlis Y. An approach to the optimization of preparation of bioprosthetic heart valves. J Biomech. 1991; 24(5):331–339. [PubMed: 1904875]

Neidert MR, Tranquillo RT. Tissue-engineered valves with commissural alignment. Tissue Eng. 2006; 12(4):891–903. [PubMed: 16674301]

Pedron S, Kasko AM, et al. Effect of heparin oligomer chain length on the activation of valvular interstitial cells. Biomacromolecules. 2010; 11(6):1692–1695. [PubMed: 20446725]

Peyton SR, Raub CB, et al. The use of poly(ethylene glycol) hydrogels to investigate the impact of ECM chemistry and mechanics on smooth muscle cells. Biomaterials. 2006; 27(28):4881–4893. [PubMed: 16762407]

Pibarot P, Dumesnil JG. Prosthesis-patient mismatch: definition, clinical impact, and prevention. Heart. 2006; 92(8):1022–1029. [PubMed: 16251232]

Ramaswamy S, Gottlieb D, et al. The role of organ level conditioning on the promotion of engineered heart valve tissue development in-vitro using mesenchymal stem cells. Biomaterials. 2010; 31(6): 1114–1125. [PubMed: 19944458]

Robinson PS, Johnson SL, et al. Functional Tissue-Engineered Valves from Cell-Remodeled Fibrin with Commissural Alignment of Cell-Produced Collagen. Tissue Eng. 2007

Rogers CI, Pagaduan JV, et al. Single-monomer formulation of polymerized polyethylene glycol diacrylate as a nonadsorptive material for microfluidics. Anal Chem. 2011; 83(16):6418–6425. [PubMed: 21728310]

Rowley JA, Madlambayan G, et al. Alginate hydrogels as synthetic extracellular matrix materials. Biomaterials. 1999; 20(1):45–53. [PubMed: 9916770]

Sacks MS, Schoen FJ, et al. Bioengineering challenges for heart valve tissue engineering. Annu Rev Biomed Eng. 2009; 11:289–313. [PubMed: 19413511]

Sales VL, Mettler BA, et al. Endothelial progenitor cells as a sole source for ex vivo seeding of tissue-engineered heart valves. Tissue Eng Part A. 2010; 16(1):257–267. [PubMed: 19698056]

Schaefermeier PK, Szymanski D, et al. Design and fabrication of three-dimensional scaffolds for tissue engineering of human heart valves. Eur Surg Res. 2009; 42(1):49–53. [PubMed: 18987474]

Schmidt D, Dijkman PE, et al. Minimally-invasive implantation of living tissue engineered heart valves: a comprehensive approach from autologous vascular cells to stem cells. J Am Coll Cardiol. 2010; 56(6):510–520. [PubMed: 20670763]

Seliktar D, Black RA, et al. Dynamic mechanical conditioning of collagen-gel blood vessel constructs induces remodeling in vitro. Ann Biomed Eng. 2000; 28(4):351–362. [PubMed: 10870892]

Seliktar D, Nerem RM, et al. The role of matrix metalloproteinase-2 in the remodeling of cell-seeded vascular constructs subjected to cyclic strain. Ann Biomed Eng. 2001; 29(11):923–934. [PubMed: 11791675]

Shinoka T, Ma PX, et al. Tissue-engineered heart valves. Autologous valve leaflet replacement study in a lamb model. Circulation. 1996; 94(9 Suppl):II164–168. [PubMed: 8901739]

Skardal A, Zhang J, et al. Photocrosslinkable hyaluronan-gelatin hydrogels for two-step bioprinting. Tissue Eng Part A. 2010; 16(8):2675–2685. [PubMed: 20387987]

Sodian R, Hoerstrup SP, et al. Early in vivo experience with tissue-engineered trileaflet heart valves. Circulation. 2000; 102(19 Suppl 3):III22–29. [PubMed: 11082357]

Sodian R, Loebe M, et al. Application of stereolithography for scaffold fabrication for tissue engineered heart valves. ASAIO J. 2002; 48(1):12–16. [PubMed: 11814091]

Sodian R, Schaefermeier P, et al. Use of human umbilical cord blood-derived progenitor cells for tissue-engineered heart valves. Ann Thorac Surg. 2010; 89(3):819–828. [PubMed: 20172137]

Sodian R, Sperling JS, et al. Tissue engineering of a trileaflet heart valve-early in vitro experiences with a combined polymer. Tissue Eng. 1999; 5(5):489–494. [PubMed: 10586103]

Sutherland FW, Perry TE, et al. From stem cells to viable autologous semilunar heart valve. Circulation. 2005; 111(21):2783–2791. [PubMed: 15927990]

Tayalia P, Mendonca CR, et al. 3D Cell-Migration Studies using Two-Photon Engineered Polymer Scaffolds. Advanced Materials. 2008; 20(23):4494–4498.

van Geemen D, Driessen-Mol A, et al. Variation in tissue outcome of ovine and human engineered heart valve constructs: relevance for tissue engineering. Regen Med. 2012; 7(1):59–70. [PubMed: 22168498]

Vesely I. Aortic root dilation prior to valve opening explained by passive hemodynamics. J Heart Valve Dis. 2000; 9(1):16–20. [PubMed: 10678371]

Xu C, Chai W, et al. Scaffold-free inkjet printing of three-dimensional zigzag cellular tubes. Biotechnology and Bioengineering. 2012 n/a-n/a.

Zhang H, Wang L, et al. Controllable properties and microstructure of hydrogels based on crosslinked poly(ethylene glycol) diacrylates with different molecular weights. Journal of Applied Polymer Science. 2011; 121(1):531–540.

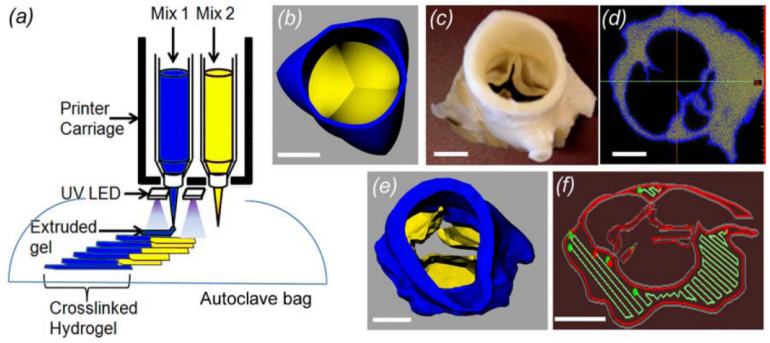

Figure 1.

3D Printer setup and valve geometry modeling. (a) Syringe tools were loaded with different hydrogels, and UV-LED array integrated into the deposition tools crosslinked hydrogels during printing. Sterile scaffolds were generated by printing inside an autoclaved bag that was mounted on the printer stage inside a laminar hood. (b) Axisymmetric valve STL file with the root and leaflet in the closed position was designed in Solidworks. (c) A fixed porcine aortic valve underwent micro-CT scan, and (d) the leaflet and root regions were thresholded based on tissue density. (e) The thresholded regions were reconstructed into printable STL geometries, (f) and the printing software sliced the geometries into layers and generated extrusion paths for each layer (red: contour, green: fill-in paths). Scale bar = 1 cm.

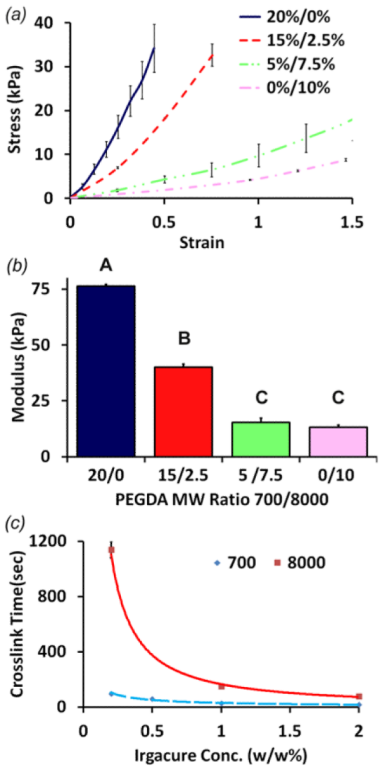

Figure 2.

Uniaxial tensile testing and crosslinking time testing of PEG-DA hydrogels. (a) Stress-strain profile, and (b) elastic modulus of hydrogels with 20:0, 15:2.5, 5:7.5, and 0:10% 700:8000 MW PEG-DA hydrogels (n = 3). Non-matching letters are statistically different ($p < 0.05$). (c) Crosslinking time of 700 and 8000 MW PEG-DA hydrogels with varying photoinitiator concentrations ($n \geq 5$).

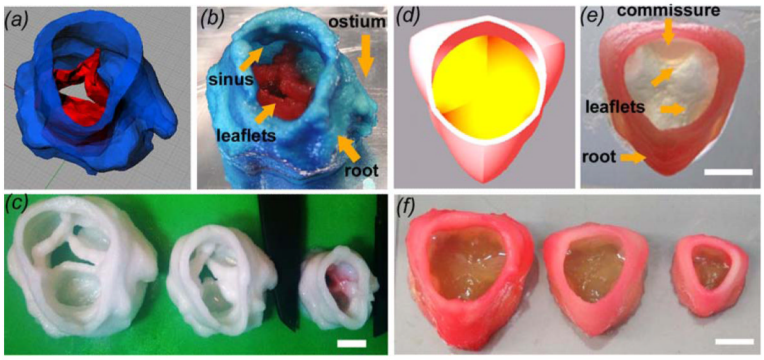

Figure 3.

Printing heterogeneous valve and scaled valve constructs. (a) Porcine aortic valve model was (b) printed, where root was formed with 700 MW PEG-DA hydrogel while the leaflets were formed with 700/8000 MW PEG-DA hydrogels. Key features such as the coronary ostium and sinuses were present (c) Scaffolds were printed with 700 MW PEG-DA at different scale for fidelity analysis, where the inner diameters (ID) were 22, 17, and 12 mm. (d) Axisymmetric valve model was (e) printed with two blends of hydrogels (f) and at 22, 17, and 12 mm ID. Scale bar = 1 cm.

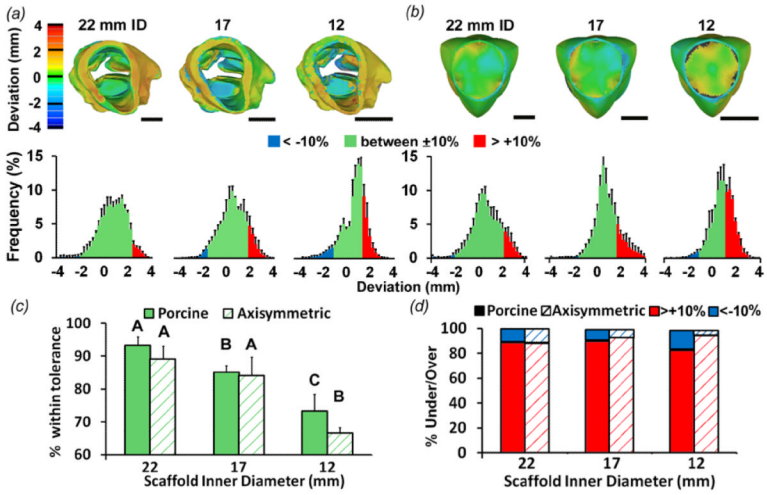

Figure 4.

Fidelity analysis of fully hydrated printed valve scaffold geometry compared to model geometry using mCT-derived STL files. (a) Heat maps and average % frequency histograms representing surface deviations between printed porcine scaffold vs. model geometries and (b) printed simplified scaffolds vs. model geometries. Printed valve constructs were fully hydrated in PBS (equilibrium swollen). Warmer colors indicate positive deviation while cooler colors indicate negative deviation in millimeters. % frequency histograms show the of deviations that lie within ±10% tolerance (green), and outside the tolerance (blue and pink). ±10% tolerance is 2.2, 1.7, and 1.2 mm for the 22, 17 and 12 mm diameter scaffolds, respectively. (c) The percentage of surface points whose deviation falls within ±10% tolerance. This percentage decreases as scaffold size decreases. Bars of the same pattern with different letters are significantly different from each other, $P<0.05$ (d) The percentage of surface points whose deviation falls outside the ±10% tolerance that are above (pink) and below (blue). Scale bar = 1 cm. n = 2-4, $p < 0.05$.

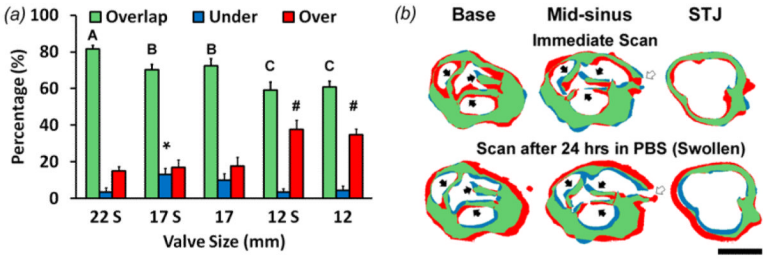

Figure 5.

Slice-by-slice analysis comparing mCT image slices of printed porcine valve scaffolds to model layers and assess internal geometric fidelity. (a) Overlap, underprint, and overprint area percentage of each printed construct. S denotes constructs that were fully hydrated in PBS (swollen), and absence of an S means constructs were scanned directly after printing. Bars of the same color with different letters or symbols are significantly different from each other, P<0.05 (b) Representative images of Boolean analysis of valve sections at levels of base, mid-sinus, and sino-tubule junction (STJ). mCT image slices of a printed scaffold are compared to slices of the native geometry used to print the scaffold. Top row: 17 mm ID valve scaffold scanned immediately after printing. Bottom: Same scaffold that was later fully hydrated. Solid arrow: leaflets; hollow arrow: ostium. N=3-4, $p < 0.05$

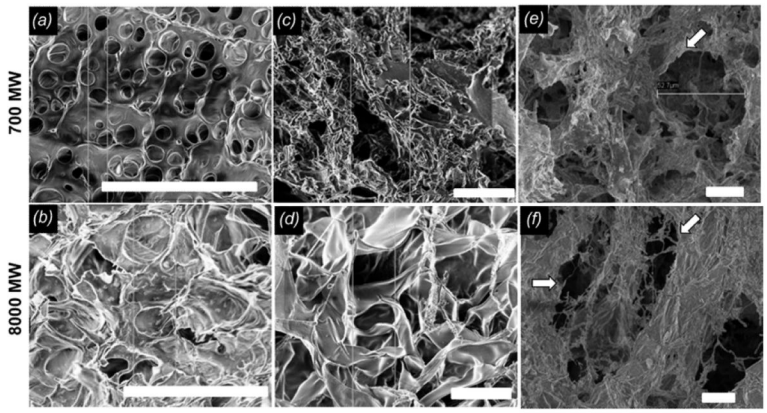

Figure 6.

Representative SEM imaging of hydrogels. Top row: 700 MW PEG-DA; bottom row: 8000 MW PEG-DA. (a, b) Images of PEG-DA hydrogels that were made with alginate viscosity modifier in the precursor solution. (c, d) Rinsed PEG-DA hydrogels made with alginate viscosity modifier (e, f) Rinsed PEG-DA hydrogels made with the addition of 0.1 mg/mL collagen and alginate viscosity modifier to precursor solution. Hollow arrows indicate fibrous material. Scale bar = 20 μm.

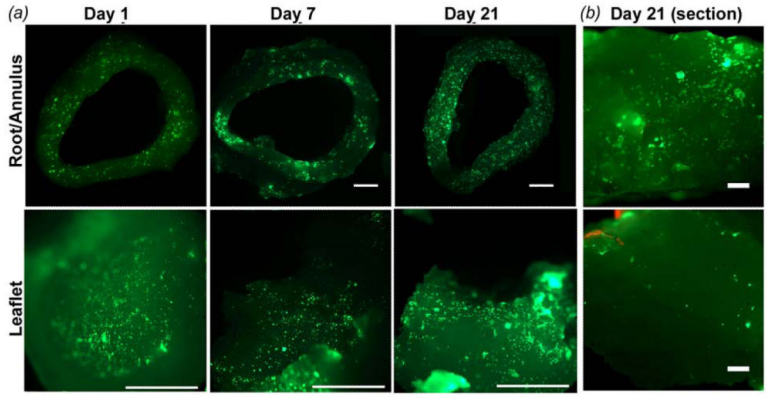

Figure 7.

Live/Dead imaging of PAVIC cultured on 12 mm ID printed valve constructs. (a) Live PAVIC were visible in both the root (top) and leaflets (bottom) surface for day 1, 7, and 21 (scale bar = 2 mm). (b) Cells were also detected in the interstitium of the root and leaflet for up to 21 days (scale bar = 100 mm).

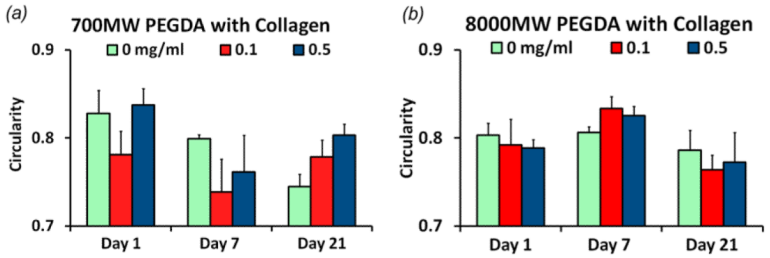

Figure 8.

Morphology of PAVIC cultured on PEG-DA and collagen hydrogels. (a) Circularity of PAVICs on 700 MW PEG-DA (control), + 0.1 mg/mL, and + 0.5 mg/mL collagen at 1, 7, and 21 days of culture. (b) Circularity of PAVIC on 8000 MW PEG-DA hydrogels with and without collagen for up to 21 days. * indicates statistical difference with $p < 0.05$.